第 34 卷第 12 期　　焊　接　学　报　　Vol. 34　No. 12
2013 年 12 月　　TRANSACTIONS OF THE CHINA WELDING INSTITUTION　　December　2013

扩散焊接钨/钒/钢体系的界面结构及力学性能

马运柱，　王艳艳，　刘文胜，　蔡青山
（中南大学 粉末冶金国家重点实验室，长沙　410083）

摘　要： 采用厚度为 0.5 mm 钒片作为中间层，在 1 050 ℃/10 MPa/1 h 的工艺条件下，对钨/钢异种材料进行扩散焊接. 采用扫描电镜、能谱仪和纳米压痕分别对接头的微观组织、元素分布及显微硬度进行分析和测试；对接头的拉伸性能进行测试，并对其断口形貌和元素分布进行分析. 结果表明，利用母材与中间层之间元素的相互扩散，可实现钨/钢材料的焊接；钨/钢焊接接头界面区由钨－钒固溶体层、未反应钒层及钒－钢扩散层 3 部分组成，其中钒－钢界面层结构为钒/VC 层/脱碳层/钢；钢/钒扩散层具有最高的显微硬度；钨/钢接头抗拉强度为 75 MPa，含脆性相 VC 的钒/钢界面是接头失效的主要断裂源.

关键词： 钨；钢；扩散焊；中间层；界面组织
中图分类号： TG456.9　　**文献标识码：** A　　**文章编号：** 0253－360X(2013)12－0017－04

马运柱

0　序　　言

偏滤器是现代磁约束核聚变装置中至关重要的组成部分，为了改善装置的屏蔽效果并提高能量转化效率，新一代示范堆聚变堆试验装置对偏滤器材料提出了更高的要求，而钨及其合金材料具有高的熔点、低的蒸气压和低的溅射腐蚀率，被认为是理想的候选材料[1]. 钨和钢物理性能特别是线膨胀系数相差比较大，在连接和部件服役过程中将产生高的热应力，导致钨/钢接头性能下降，严重降低偏滤器寿命. 近年来国外对钨/钢焊接做了大量研究，国内由于起步较晚，却鲜有报道. 目前钨/钢连接采用的焊接方法主要是钎焊[2,3]和扩散焊[4－6]，扩散焊具有连接温度低，焊件受热面积小，易获得性能优异的异种材料连接接头等优点而受到广泛关注[7,8].

在扩散焊焊接过程中，常常通过添加中间层来缓解接头残余应力，提高材料使用寿命. 目前采用的中间层主要是纯金属箔带，包括镍[9]、铌[5]、钛[6]等. 钒的线膨胀系数置于钨与钢之间，且与钨、钢均能形成连续固溶体，采用钒作为钨/钢焊接中间层不仅可缓解接头的残余应力，还可避免有害相的生成；另外钒具有良好的结构强度和低的裂变中子吸收截面，在核领域中广泛应用，因此钒是钨/钢焊接理想的中间层材料. 文中以钒片为中间层，在 1 050 ℃温度下进行钨/钢扩散焊接，并对焊接接头的微观组织演变、力学性能及断裂特征进行研究.

收稿日期： 2012－09－03
基金项目： 国家自然科学基金资助项目(50774098)；国家 863 高技术研究发展计划资助项目；教育部"长江学者特聘教授"奖励计划

1　试验方法

试验所采用的材料为工业用纯钨棒(纯度 99.9%)和铁素体钢(ferrite steel，FS)，中间层材料是厚度为 0.5 mm 的钒片，纯度为 99.9%. 分别将纯钨棒和钢材加工成直径为 35 mm，长为 13 mm 的圆柱形焊接试样，将待焊表面用 180 号、400 号、800 号、1 000号、1 200 号、1 500 号金相砂纸逐级打磨并抛光，随后分别置于丙酮和酒精中超声清洗 20 min，冷风吹干备用.

焊接试验在 HI-MVLTI-10000 型真空热压机中进行，工作环境为真空，包套为石墨模具，焊接试样装配如图 1 所示.

采用的扩散焊工艺条件如表 1 所示. 焊接完成后，对焊接试样的焊接界面进行取样，经打磨、抛光后，采用 Novatm Nano SEM230 型扫描电镜观察接头界面组织和形貌，用扫描电镜上自带的能谱仪进行接头元素分析；采用 VNHT 型纳米压痕仪测试接头显微硬度，试验所施加的最大载荷为 30 mN.

将焊接试样线切割成标准拉伸试样(图 2)，用美国 Instron3369 力学试验机测试接头抗拉强度，并

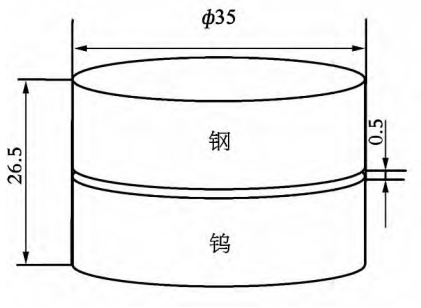

图 1 扩散焊接头示意图 (mm)

Fig. 1 Schematic of assembling joint

表 1 扩散焊工艺参数

Table 1 Parameters of diffusion bonding

焊接温度	保温时间	焊接压力	真空度
T/K	t/h	p/MPa	α/Pa
1 323	1	10	$<10^{-3}$

采用扫描电镜及能谱仪对拉伸断口进行观察和元素分析.

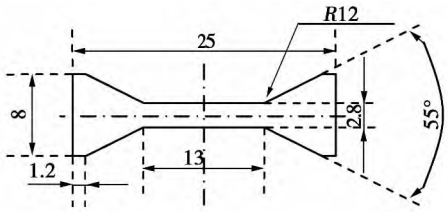

图 2 标准拉伸试样图(mm)

Fig. 2 Schematic of standard tensile specimen

2 试验结果与讨论

2.1 界面结构与分析

图 3 为钨/钢扩散焊接头的 SEM 形貌,焊接接头存在两个明显的扩散界面,分别为钨/钒和钒/钢界面. 从图 3 可知,钨/钒/钢的焊接界面结合致密、分布均匀,未发现明显的裂纹等缺陷,说明采用钒作中间层可以实现钨与钢的焊接.

2.1.1 钨/钒界面分析

图 4a 为钨/钒界面的高倍组织形貌. 可以看出,钨/钒界面扩散层非常薄,这可能与钨和钒的熔点均较高、在 1 050 ℃的焊接温度下无法激活钨与钒的真空扩散有关,导致钨/钒界面处元素扩散较慢,扩散层较薄. 对钨/钒界面处元素 W 和 V 分别进行线扫描(位置如图 4a 横线所示) ,如图 4b 所示,钨/钒界面扩散层厚度约为 2 μm,界面处元素分布曲线平滑,无明显台阶,说明此界面处元素分布连续性好,无金属间化合物的生成和聚集. 另外由 W-V 二元相图可知,钨与钒在液态及固态下可形成连续固溶体,因此可以推断钒/钨界面处形成的是约 2 μm 厚的钒(钨) 固溶体层.

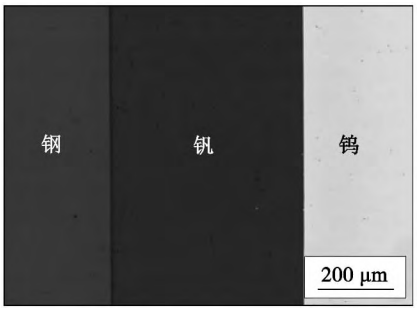

图 3 钨/钢扩散焊接头界面形貌

Fig. 3 Interfacial microstructure of W/FS joint

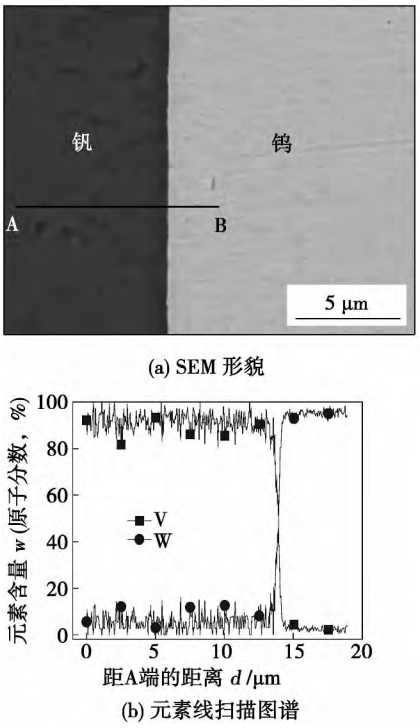

图 4 钨/钒界面

Fig. 4 W/V interface

2.1.2 钢/钒界面分析

图 5a 为钢/钒界面的高倍组织形貌. 可以看出,钢/钒界面处存在一定厚度的反应层(深色部分) . 对 Fe 和 V 元素进行线扫描(位置如图 5a 横线所示) ,如图 5b 所示,在钢/钒界面形成了约 5 μm 厚的扩散层,元素分布曲线平滑且无明显台阶,说明 Fe 与 V 元素未形成金属间化合物. 对扩散层进行点扫描分析,发现了 C 元素的存在,且与 V 元素的

原子比接近 1∶1，从中间层相的颜色和形态判断，形成了碳化钒晶体，其中碳来源于界面附近钢中碳元素向钒中间层的扩散，而近界面钢的一侧形成了脱碳层.

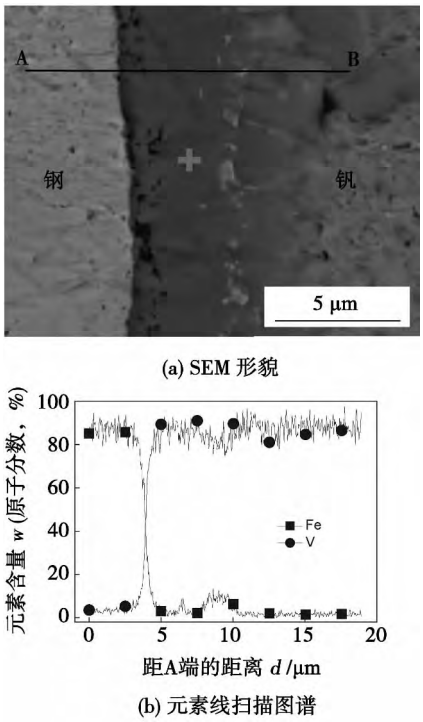

(a) SEM 形貌

(b) 元素线扫描图谱

图 5　钢/钒界面结构

Fig. 5　FS/V interface

钢/钒界面层的形成及长大过程可分为 3 个阶段. (1) 物理接触阶段. 该阶段主要是表面的微观凸起部分在大的焊接压力作用下产生塑性变形，使界面达到紧密接触、界面区原子处于激活状态，为后续原子扩散做准备. 此阶段原子几乎没有扩散，无反应层出现. (2) VC 及脱碳层形成阶段. 随着焊接过程的进行，钢中的 Fe，C 等元素向中间层钒中扩散，中间层元素 V 则向钢中扩散. 由于 Fe 和 V 原子半径相近，互扩散能垒大，扩散速度慢，在一定时间内，形成的扩散层厚度有限. 但 C 原子半径小，扩散速度快，在钒侧的界面处生成 VC 晶核，并生长为 VC 层. 同时由于碳的大量扩散，近界面钢侧的微小区域内出现了贫碳现象，形成脱碳层. 因此此时的界面结构变为钒/VC 层/脱碳层/钢. (3) 反应层的成长阶段. 随着焊接过程的继续进行，元素进一步扩散，VC 层与脱碳层厚度不断变大[10].

从图 5a 还可以看出，界面处靠近中间层钒侧存在一定数量的孔隙. 这一方面是因为钢中的 C 元素向钒中间层扩散，与钒生成疏松状的 VC 粗晶粒相，致使在钢/扩散层界面产生了孔隙. 另一方面与中间层的 V 元素向钢中扩散有关. 据文献报道，V 元素在钢中的扩散系数大于 Fe 元素在钒中的扩散系数[10]；同时高温下元素在基体中的体扩散和晶界扩散速度差别很小，而钒的熔点比钢要高得多，因此 1 050 ℃时钒向钢基体中扩散更易发生，从而在界面处靠近钒中间层一侧产生了孔隙.

2.2　界面显微硬度分析

图 6 为显微硬度分析曲线. 图 6a 为焊接界面不同区域(分别为钨、钒(钨)固溶体、钒、钒/钢扩散层(diffusion zone，DZ)和钢(FS))纳米压痕试验所得载荷—位移曲线. 由 6 图可知，在施加相同载荷的情况下，不同区域压痕深度不一样，各区域压痕深度值分别为：钒层(880 nm)、钒(钨)固溶体层(680 nm)、钢(640 nm)、钨(500 nm)、钒/钢扩散层(300 nm). 一般来说压痕越浅，材料硬度越高，因此钒/钢扩散层硬度最高，而钒中间层硬度最低.

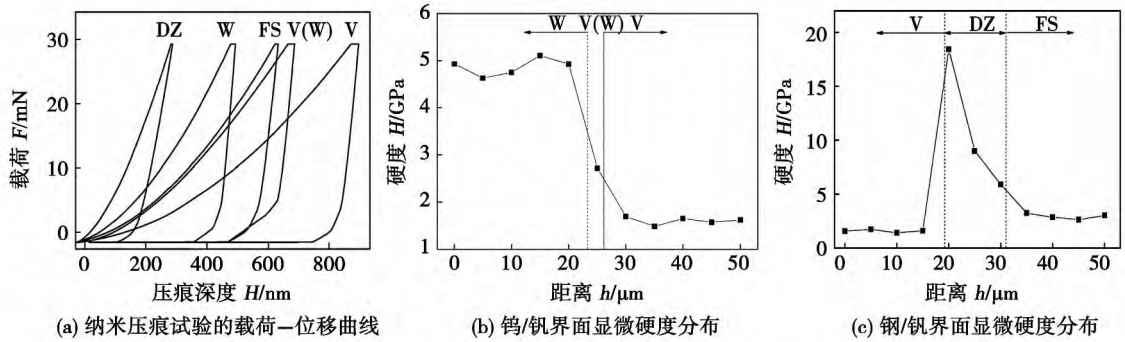

(a) 纳米压痕试验的载荷—位移曲线　(b) 钨/钒界面显微硬度分布　(c) 钢/钒界面显微硬度分布

图 6　界面显微硬度分析

Fig. 6　Hardness distribution along cross-section of W/FS joint

图 6b，c 为钨/钢扩散焊接头显微硬度分布，可清晰看到钨/钢界面、钢/钒界面的显微硬度趋势. 由于 W 与 V 的相互扩散，钨/钒界面处钒(钨)固溶体的硬度置于母材钨与中间层钒之间，如图 6b 所

示. 但是钢/钒界面处扩散层的硬度远远大于母材，如图 6c 所示. 结合钢/钒界面成分分析，此反应层中有化合物碳化钒生成. 一般来说在钢铁和硬质合金中添加碳化钒能提高材料的硬度等综合性能，因此，在钢/钒界面扩散层中高硬脆相碳化钒的生成明显提高了接头的硬度. 同时由二元相图知，铁与钒可能形成固溶体，V 原子与 Fe 原子尺寸不同，形成固溶体后，基体晶格发生畸变，增加位错运动的阻力，也能使得材料的硬度值有所提高.

2.3 焊接接头拉伸性能及断口分析

钨/钒/钢接头抗拉强度约为 75 MPa，抗拉强度偏低且波动性较大，这可能与高温焊接后接头内残余应力较大有关，此外焊接后的线切割操作也会对接头性能有一定的影响. 从宏观上看，试样的断裂主要发生在钒/钢界面，断口形貌如图 7 所示，断裂方式为典型的脆性断裂. 对断口进行能谱分析，铁含量很少，V 和 C 原子比接近 1∶1，结合界面成分分析，此处为 VC 层，因此在钒/钢界面发生脆断的原因主要是界面扩散层内形成了大量的脆性碳化钒相. 生成碳化钒的反应进行比较充分，厚度较大，界面硬度虽然很高，但由于脆性相的生成而成为接头的薄弱部位，使接头处的应力分布变得更加复杂，从而使接头强度较低. 另外可能与焊接后界面处残留的孔隙有关. 因此阻止高硬脆相碳化物、残留孔隙的生成(如选择非碳化物形成元素作为中间层材料)，可有效提高接头的拉伸性能.

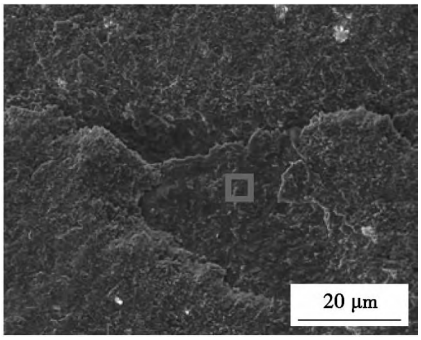

图 7 钨/钢扩散焊接头断口形貌及 EDS 分析结果

Fig. 7 Fracture appearance and EDS analysis results of W/FS joint

3 结 论

(1) 钨/钢焊接接头界面区由钒(钨)固溶体层、未反应钒层、钒 - 钢扩散层组成，实现了钨/钢连接.

(2) 固溶体钒(钨)相的存在，提高了钨/钒界面扩散区的显微硬度; 高硬脆相 VC 晶粒的生成大大. 提高了钒/钢界面的显微硬度.

(3) 钨/钒/钢扩散焊接头抗拉强度为 75 MPa，接头断裂失效主要发生在有脆性相 VC 生成的钒/钢界面，属于脆性断裂模式.

参考文献:

[1] 郭双全，冯云彪，燕青芝，等. 偏滤器中钨与异种材料的连接技术研究进展[J]. 焊接技术，2010，39(9)：3 - 7.
Guo Shuangquan，Feng Yunbiao，Yan Qingzhi，*et al*. Development of joining technologies on tungsten with dissimilar materials for divertor [J]. Welding Technology，2010，39(9)：3 - 7.

[2] Kalin B A，Fedotov V T，Sevrjukov O N，*et al*. Development of brazing foils to join monocrystalline tungsten alloys with ODS-EUROFER steel [J]. Journal of Nuclear Materials，2007，367：1218 - 1222.

[3] Kalin B A，Fedotov V T，Sevrjukov O N，*et al*. Development of rapidly quenched brazing foils to join tungsten alloys with ferritic steel [J]. Journal of Nuclear Materials，2004，329：1544 - 1548.

[4] Zhong Zhihong，Jung Hunchea，Hinoki Tatsuya，*et al*. Effect of joining temperature on the microstructure and strength of tungsten/ferritic steel joints diffusion bonded with a nickel interlayer [J]. Journal of Materials Processing Technology，2010，210(13)：1805 - 1810.

[5] Basuki W W，Aktaa J. Investigation of tungsten/EUROFER97 diffusion bonding using Nb interlayer [J]. Fusion Engineering and Design，2011，86(9)：2585 - 2588.

[6] Zhong Zhihong，Hinoki Tatsuya，Nozawa Takashi，*et al*. Microstructure and mechanical properties of diffusion bonded joints between tungsten and F82H steel using a titanium interlayer [J]. Journal of Alloys and Compounds，2010，489(2)：545 - 551.

[7] 周 媛，熊华平，陈 波，等. 以铜和 Cu-Ti 作为中间层的 TiAl/GH3536 扩散焊[J]. 焊接学报，2012，33(2)：17 - 20.
Zhou Yuan，Xiong Huaping，Chen Bo，*et al*. Diffusion bonding of TiAl and GH3536 superalloy with Cu and Cu-Ti as interlayers [J]. Transactions of the China Welding Institution，2012，33(2)：17 - 20.

[8] 李卓然，于 康，刘 兵，等. GH4169 合金真空扩散连接接头的组织与性能[J]. 焊接学报，2010，31(11)：13 - 16.
Li Zhuoran，Yu Kang，Liu Bing，*et al*. Microstructure and properties of GH4169 vacuum diffusion bonded joint [J]. Transactions of the China Welding Institution，2010，31(11)：13 - 16.

[9] 何 鹏，李海新，林铁松，等. TiAl 合金与镍基高温合金的扩散连接[J]. 焊接学报，2012，33(1)：17 - 20.
He Peng，Li Haixin，Lin Tiesong，*et al*. Diffusion bonding of TiAl and Ni-based superalloy [J]. Transactions of the China Welding Institution，2012，33(1)：17 - 20.

[10] Le Claire A D，Neumann G. Landolt-böornl numerical data and functional relationships in science and technology-group III condensed matter [M]. Berlin：Springer，2006.

作者简介: 马运柱，男，1975 年出生，博士，教授. 主要从事电子封装材料、难熔金属材料方面的科研和教学工作，发表论文 50 余篇.
Email：zhuzipm@csu.edu.cn

MAIN TOPICS, ABSTRACTS & KEY WORDS

Detection of seam deviation of micro butt gap in laser welding of 304 austenitic stainless steel based on corner point method GAO Xiangdong, HUANG Jianyuan, MO Ling (School of Electromechanical Engineering, Guangdong University of Technology, Guangzhou 510006, China). pp 1 – 4

Abstract: Infrared radiation from the molten pool contains plenty of welding status information including the characteristics of the seam deviation. Infrared images of the molten pool were captured by an infrared sensitive high-speed camera during high power (10kW) fiber laser butt joint welding of 304 austenitic stainless steel with micro-gap seam (seam gap width was less than 0.1mm). By analyzing the molten pool characteristics, the information of seam deviation was explored. A keyhole formed when the laser beam was focused on a weldment and the metal vaporized instantly. Features of the keyhole infrared images, especially the characteristics of conjunction between the solid and liquid zones with unstable burr edge of seam were studied. A corner point detection method was proposed to detect the micro-gap seam deviation in high power laser welding process. Experimental results showed that the dense distribution center of the corner points of a molten pool infrared image had a close relationship with the weld seam deviation. The micro-gap weld seam deviation status in high power fiber laser welding can be determined by the corner point distribution density.

Key words: high power fiber laser welding; near infrared thermal image; seam deviation; corner point detection

Embedded system control of consumable DE-GMAW SHI Yu[1], WANG Ping[2], GUO Jinchang[2], FAN Ding[1] (1. State Key Laboratory of Gansu Advanced Non-ferrous Metal materials, Lanzhou University of Technology, Lanzhou 730050, China; 2. Welding Team of Process Department in Dongfang Electrical Machinery Co., Ltd., Deyang 618000, China). pp 5 – 8

Abstract: By applying the embedded system control to carry out the control tests for consumable DE-GMAW, the welding process is unstable, main arc and bypass arc are affected each other, bypass arc length is unstable, bypass current changes seriously, and there is welding defects and poor weld appearance in open loop welding. Stability test of the welding process based on the arc voltage feedback prove that the embedded system can feedback arc voltage in real time, adjust bypass wire feeding rate and control the bypass arc length, make sure welding process stable. Stability test of the welding process based on the current control shows that the embedded system can feedback the bypass current in real time, judge the bypass current change trend, adjust the bypass current in real time, ensure current in base metal to be stable. Applications of the embedded system control of both bypass wire feeding and bypass current ensure stable welding process, avoidiance of welding defect and good weld appearance.

Key words: embedded system; consumable DE-GMAW; arc voltage feedback; control current

Parameter optimization for MAG of DP780 LU Zhenyang, TANG Chao, XIONG Wei, HUANG Pengfei (Welding Institute, Beijing University of Technology, Beijing 100124, China). pp 9 – 12

Abstract: Gas metal arc welding parameters were optimized by orthogonal experiments for 2mm thick uncoated DP780 steel plate. The influences of five factors including wire feeding rate, welding speed, arc voltage, wire extension and welding angle on tensile strength of DP780 lap joints were discussed. The range analysis and variance analysis proved that wire feeding rate and welding speed are the main influencing factors on the tensile strength of the join, and the other factors show no regularity to tensile strength. An approximate mathematical model to control the tensile strength of the joint was obtained by fitting the proximate curve through multiple regression analysis, which revealed the regularity of effects of main welding parameters on the tensile strength of the joint.

Key words: AHSS; MAG; process parameter optimization

A welding power supply with half-bridge LLC resonant soft-switching CHEN Yanming[1], YANG Meizhen[1], WANG Zhenmin[2], XUE Jiaxiang[2], LI Guojin[1] (1. College of Electrical Engineering, Guangxi University, Nanning 530004, China; 2. College of Mechanical Engineering, South China University of Technology, Guangzhou 510640, China). pp 13 – 16

Abstract: By using the magnetizing inductance of transformer, resonant capacitor and additional inductance, a half-bridge LLC resonant welding power supply with constant output voltage was implemented. Through careful analysis and design of relevant parameters (such as the series resonant inductor Lr, series resonant capacitor Cr, and the resonant inductor Lm paralleled with transformer etc) in the resonant tank, the ZVS turn-on can be achieved for primary side power switch, and the ZCS turn-off can be achieved for secondary rectifier diodes over the entire operation region. Hence, the loss and the interference can be decreased, the efficiency can be increased, the switching frequency can be higher so that the weight and the volume of the inductance, the capacitance and the transformer, and so on, can be decreased dramatically, and the dynamic behavior can be improved. The operation principle was also discussed briefly, a 2.5kW half-bridge LLC welding power supply was constructed and the experimental results were presented.

Key words: half-bridge LLC converter; resonant; Zero-voltage turn-on; Zero-current turn-off

Interface microstructure and mechanical properties of diffusion bonded joints between tungsten and ferritic steel with vanadium interlayer MA Yunzhu, WANG Yanyan, LIU

Wensheng, CAI Qingshan (State Key Laboratory for Powder Metallurgy, Central South University, Changsha 410083, China). pp 17 – 20

Abstract: The interface characteristics between W and ferrite steel (FS) diffusion welded with a V interlayer of 0.5mm in thickness was investigated in vacuum hot pressing furnace at 1 050 ℃ for 1h and 10 MPa. Microstructures, element compositions and micro-hardness of joint were analyzed and tested with field-emission scanning electron microscopy (FE-SEM), energy dispersive spectroscopy (EDS) and nanoindenter, respectively. Tensile strength was tested with mechanical test machine. Results showed that, a reliable bonding on W/FS interfaces by means of diffusion welding between matrix and V interlayer was obtained. The W/FS joint is a multilayer sandwich structure, which includes the transition zone of W/V, the residual V interlayer and the diffusion layer of V/FS. Meanwhile, the transition zone of W/V was mainly composed of a solid solution structure and the V/FS diffusion layer with the highest hardness where there was a definite structure of V/VC layer/decarburized layer/FS. The tensile strength of joint reaches 75MPa and V/FS interface is main fracture source because of containing brittle VC phase.

Key words: tungsten; steel; diffusion bonding; interlayer; microstructure

Elimination of lazy S defect in friction stir welded joint of 20mm-6063 alumimum alloy HE Diqiu, YE Shaoyong, WANG Jian (State Key Laboratory of Complicated Equipment Design and Extreme Manufacturing, Central South University, Changsha 410083, China). pp 21 – 24

Abstract: 20 mm thick 6063 aluminum alloy plate were joined by friction stir welding with gas protection. The result showed that the sound joint without lazy S can be achieved. The average tensile strength of welds is 148.9 MPa, which is 81.9% of that of the base metal. Optical microscopy revealed the stir zone presents particularly fined equiaxed gains formed by dynamic recrystallization. The microstructure in TMAZ, in which some degree of dynamic recrystallization occurs, consists of deformed gains. The result shows that lazy S of 6063 aluminum alloy can be eliminated by FSW with gas protection.

Key words: friction stir welding; 6063 aluminum alloy; lazy S; microstructure

A novel method of in-situ fabrication of Mg surface composites by friction stir process HUANG Yongxian[1], WANG Tianhao[1], LÜ Shixiong[1], LIU Huijie[1], AO Feng[2] (1. State Key Laboratory of Advanced Welding and Joining, Harbin Institute of Technology, Harbin 150001, China; 2. Yangzhou Qiuyuan Pressure Vessel Manufacturing Co., Ltd., Yangzhou 225115, China). pp 25 – 28

Abstract: In the previous fabrication process of surface composite by friction stir process (FSP), the reinforcement phases were needed to preplace on the base metal. However, these particles didn't distribute very well in the stir zone. Therefore, friction stir process without preplacing reinforcement phase was proposed to prepare the surface composite. A FSP tool consisting of only shoulder was designed, and used to fabricate the surface composite on the AZ31 plate as-rolled. Microstructure was analyzed by optical microscope and SEM. The microhardness and surface wear resistance tests of specimens show that the particle reinforcement are more homogeneous, so that the microhardness and wear resistance increase, and at the same time, the preparation work is simplified to a great extent.

Key words: magnesium alloy; friction stir process; in-situ; surface composites

Characteristics of bypass-current MIG-TIG double-sided welding of stainless steel MIAO Yugang[1], HAN Duanfeng[1], WU Bintao[2], XU Xiangfang[2], LI Xiaoxu[2] (1. National Key Laboratory of Science and Technology on Underwater Vehicle, Harbin Engineering University, Harbin 150001, China; 2. College of Shipbuilding Engineering, Harbin Engineering University, Harbin 150001, China). pp 29 – 32

Abstract: By using 6mm thick 304 stainless steel plate as base metal, the bypass-current double-sided arc welding experiments were carried out. The results showed the technology can obtain the stable process and good weld appearance. The other remarkable advantages such as increasing joint penetration, deceasing welding defects, enhancing production efficiency, reducing welding cost were also achieved. The reliable joining of 6mm thick 304 stainless steel was realized at welding current of 110 A. Furthermore, the melting efficiency of bypass-current double-sided arc welding can reach 60.2%, more than 17.6% of TIG welding and 43.2% of bypass-current MIG welding. The tensile results showed the strength of the joints can reach 776.5MPa, about 95% of that of base metal. The fracture occurs at the heat-effect zone, and the angle between fracture line and stress direction is 45°. The fracture appearance is gray, which shows the characteristics of ductile fracture.

Key words: bypass-current MIG-TIG double-sided welding; melting efficiency; tensile strength; weld appearance

Test and analysis of arc pressure measurement in coupling arc electrode TIG welding HUANG Yong[1,2], HAO Yanzhao[2], QU Huaiyu[2], LIU Ruilin[2] (1. State Key Laboratory of Gansu Advanced Non-ferrous Metal Materials, Lanzhou University of Technology, Lanzhou 730050, China; 2. Key Laboratory of Non-ferrous Metal Alloys and Processing, The Ministry of Education, Lanzhou University of Technology, Lanzhou 730050, China). pp 33 – 36

Abstract: A kind of coupling arc tungsten electrode was developed to decrease arc pressure remarkably, avoid undercut and humping weld. Adopting this method, high-quality TIG welding with relative higher speed can be achieved. The TIG arc pressure of this kind of welding process was tested to investigate the influence of the parameters on distribution of arc pressure. Compared with the traditional TIG arc, the TIG arc pressure with coupling arc electrode is much lower with the same parameters, and decreases with the increase of arc length, the increase of electrode extended length, the decrease of current, the increase of the electrode gap width and the increase of the electrode diameters. The arrangement of the influence in decreasing order is current, electrode extended length, arc length and electrode diameter, electrode gap width.